



# Combination of Surface Plasmon Polaritons and Subwavelength Grating for Polarization Beam Splitting

Yuan Xie<sup>1</sup> · Zhenxing Chen<sup>1</sup> · Jun Yan<sup>1</sup> · Yiheng Wu<sup>1</sup> · Tianye Huang<sup>1</sup>  · Zhuo Cheng<sup>1</sup>

Received: 2 July 2019 / Accepted: 3 September 2019 / Published online: 12 September 2019  
© Springer Science+Business Media, LLC, part of Springer Nature 2019

## Abstract

A polarization beam splitter (PBS) based on the plasmonic subwavelength grating (PSWG) is proposed and investigated. The PBS is composed by a directional coupler with a PSWG as the coupling region, which offers additional freedom for index tailoring. The mode properties are strongly modified by the unique structure of the PSWG resulting in selective coupling with the two polarization states in the neighbor waveguides. The calculations show that the insertion loss of PBS is less than 1 dB, and the extinction ratios of transverse electric and transverse magnetic polarizations are as high as 27 dB and 30 dB respectively with nearly 4- $\mu\text{m}$  coupling region length. In addition, the fabrication tolerance of the device is investigated in detail.

**Keywords** Waveguide · Subwavelength structures · Polarization beam splitter

## Introduction

Polarization beam splitter (PBS), which separates two orthogonally polarized light beams, is an significant component for photonic integrated circuits (PICs). PBS owning the properties of compact size, high extinction ratio (ER), and low insertion loss (IL) is suitable for developing a new generation PICs [1]. Waveguide-type PBSs are designed in various ways, such as photonic crystal (PhC) [2], directional couplers (DCs) [3, 4], multimode interference (MMI) [5], and grating [6–8]. Among these structures, the DC takes the advantages of easy fabrication and flexible design.

With the rapid development of nanomanufacturing technology, subwavelength gratings (SWGs) have gathered significant attention as a promising replacement of traditional dielectric waveguides. The wavelength of light propagating through the SWG is typically much larger than its pitch [9]. Benefiting from its unique properties, e.g., effective diffraction suppression, index-engineering, and homogenous behavior [10], SWGs have been successfully applied to many devices such as high-speed modulator [11], power splitter [12],

and fiber-to-chip grating couplers [13]. Moreover, SWGs can also be a good choice for constructing PBS [14, 15]. However, in SWG-based PBS, a tapered region is usually required to ensure adiabatic transition between the SWG mode and the conventional waveguide mode due to the longitudinal variation of its structure.

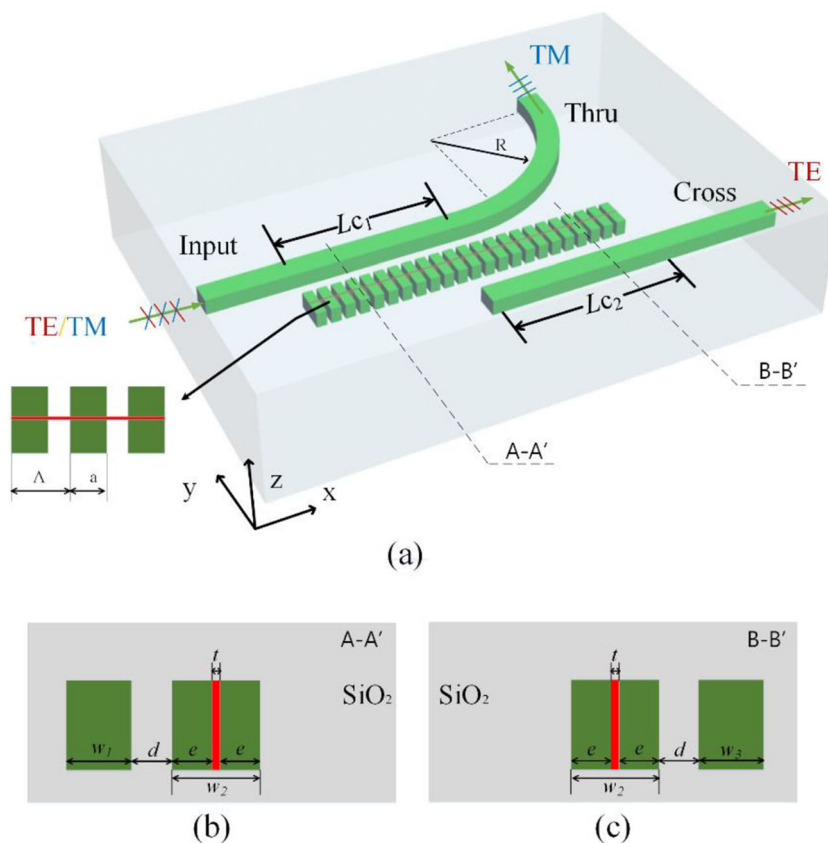
Surface plasmon polaritons (SPPs) propagate on the interface between metal conductor and a dielectric in the form of electromagnetic waves. Its characteristics are used to manipulate and guide optical signals in PICs [16]. In recent years, candidate methods based on SPP at the interface between metals and dielectric materials have been considered to achieve polarization beam splitting. For example, a simplified ultrashort PBS using an asymmetrical coupler consisting of a silicon nanowire and a hybrid plasmonic waveguide is proposed [17], which provides an unconventional approach for operating polarization sensitivity of light in integrated circuits. Compared with pure silicon-based devices [18], the SPP-based devices provide compact size [19]. This is due to the high birefringence induced by the SPP mode, whose polarization state is usually perpendicular to the metal-dielectric interface. Particularly, the use of hybrid long-range SPP (LRSPP) waveguides results in lower propagation loss. In previous work [20], triple waveguide structure with SWG is used for separating the two modes; due to the divergence between transverse electric (TE) and transverse magnetic (TM) modes, 7- $\mu\text{m}$  coupling length is required. In order to further reduce the footprint of the device, the combination of SWG and LRSPP can be a potential solution. This is because the

✉ Tianye Huang  
tianye\_huang@163.com

✉ Zhuo Cheng  
chengzhuo@cug.edu.cn

<sup>1</sup> School of Mechanical Engineering and Electronic Information, China University of Geosciences (Wuhan), Wuhan, China

**Fig. 1** Schematic of the proposed PBS. **a** The 3D view, and the cross-sectional view of the **b** first and **c** second coupling regions



plasmonic mode can only exist in one polarization, which will induce significant difference between the two orthogonal modes and the coupling length is consequently shortened.

In this paper, a high-performance PBS assisted by plasmonic SWG (PSWG) is designed. The PBS employs a three-waveguide directional coupler (TWDC) structure composed of one metal-embedded PSWG and two conventional silicon waveguides. Due to the formation of the LRSPP mode in the PSWG, the coupling of the Bloch mode in the PSWG waveguide and TE mode in silicon waveguide is enhanced, and the TM mode in the PSWG is tailored be of large phase mismatch with the

ones besides, which lead to shorter device length and effective separation of the two polarization states. Since the PSWG is spatially separated from the output waveguide, the device does not require an additional tapered region. Finally, we investigated the impacts of coupling length, metal thickness, operation wavelength, and metal position offset on the performance comprehensively. The combination of PBS and PSWGS enriches the application field of SPPs.

**Design Principle**

The proposed PBS is formed in 340-nm silicon-on-insulator (SOI) wafer [21] using 2- $\mu$ m finite box [22]. Figure 1 indicates the three-dimensional representation of the proposed PBS, a top view of a PSWG waveguide, and cross-sectional views of two coupling regions along the direction of propagation. The whole device is covered by silica, and the refractive indices of Si and SiO<sub>2</sub> are  $n_{Si} = 3.476$ ,  $n_{SiO_2} = 1.444$ , and  $n_{Ag} = 0.1453 + 11.3587i$  [23] at 1550 nm, respectively. The dimensions of PBS are optimized so that the TE mode couples to PSWG and then to Cross port, while the injected TM mode directly outputs from Thru port. The Cross and Thru ports are conventional silicon stripe waveguides. A PSWG,

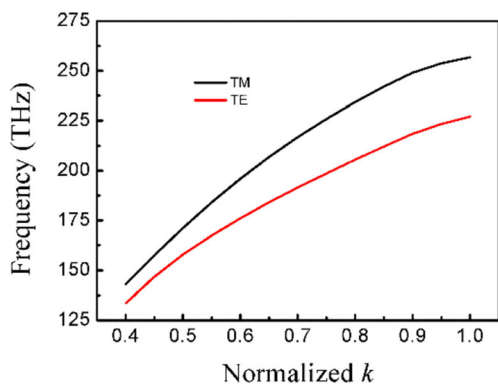
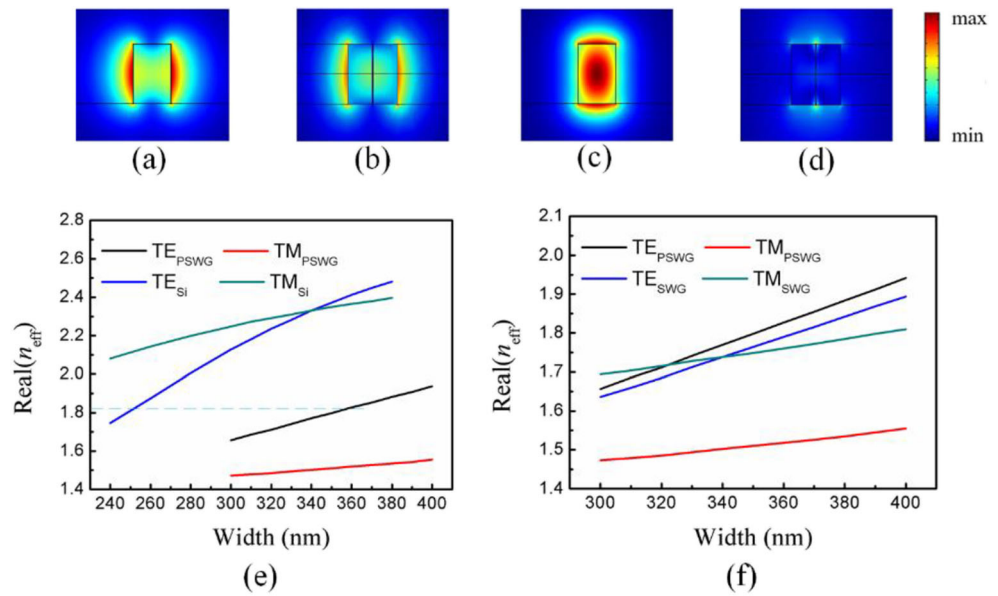


**Fig. 2** Dispersion diagram of PSWG waveguide with longitudinal propagation (along the X axis)

**Fig. 3** Field profiles of TE and TM mode in **a, c** silicon waveguide and **b, d** PSWG. The real parts of the refractive indices in silicon and PSWG (**e**), SWG, and PSWG **f** depending on different width



which is constructed by a thin Ag film embedded in a traditional SWG, is placed in the middle of the two silicon waveguides as the coupling region. The two conventional silicon waveguides are of equal width ( $w_1 = w_3$ ) in order to make the TE mode symmetrically coupled twice. The thickness of Ag film and the total width of PSWG are denoted by  $t$  and  $w_2$ , respectively. The pitch and duty cycles of the PSWG are  $\Lambda$  and  $a/\Lambda$  (the medium with higher refractive index per pitch has a length  $a$ ), respectively.

For SWG waveguides at 1550 nm, if  $\lambda/\Lambda > 2 n_B$  ( $n_B$  is the effective refractive index of Bloch mode) are satisfied, according to the effective medium theory, the PSWG can be approximately considered as a longitudinal invariant waveguide [24]. In our design,  $\Lambda$  and  $a$  is set to be 300 and 210 nm, respectively.

The Thru port has a  $90^\circ$  bend with a radius of  $R$  to decouple the fields, and  $R$  is optimized to  $3 \mu\text{m}$  so as to reduce the bending loss. Although smaller gap between two waveguides can improve coupling efficiency and shorten device length, too small gap could bring complex fabrication process. Here the gap size  $d$  between the silicon waveguide and the PSWG is

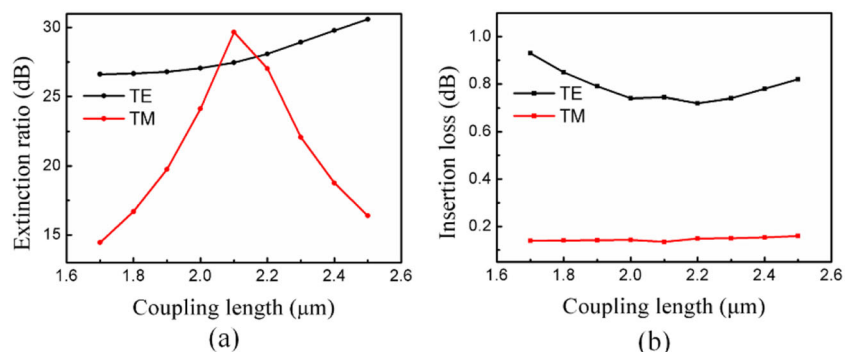
fixed at 200 nm, which is based on 248 nm optical lithography technology [25].

Figure 2 shows a schematic diagram of the dispersion relationship of a PSWG waveguide. For both orthogonal polarization modes, the frequency is monotonically increasing with the propagation constant ( $k$ ), which indicates that the PSWG waveguide behaves the same as a conventional waveguide.

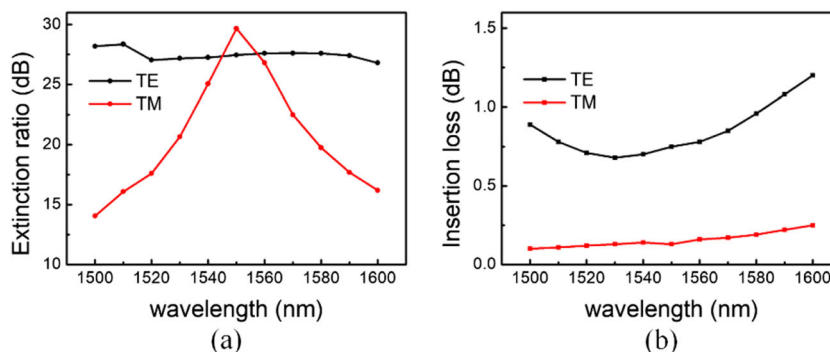
The field distribution of the two modes in different waveguides calculated by finite element method is illustrated in Fig. 3a–d. The field distribution of TE mode is very similar in two different waveguides (Fig. 3a, b). For PSWG with Si-Ag-Si structure, because the metal strip at its center supports TE polarization surface wave, a strong field enhancement effect was shown at the metal-dielectric interface. For the TM polarization, the SPP mode is not excited, and the existence of Ag thin film significantly modified the field distribution, resulting in a relatively low field distribution in the center of the waveguide (Fig. 3c, d).

By tailoring the waveguide width, the phase matching degree of the TE mode in the two waveguides is maximized, as

**Fig. 4** The relevance between ER (**a**) and IL (**b**) and coupling length



**Fig. 5** TE and TM modes of ER (a) and IL (b) at different wavelengths



shown in Fig. 3e. It can be found that in both waveguides, the effective index of the TE mode is closer comparing to the ones of TM modes. With  $w_1 = 250$  nm and  $w_2 = 355$  nm, the real effective indices of the TE modes in conventional waveguides and PSWG are substantially equal to 1.809 and 1.806, respectively, while for TM mode, the real effective refractive indices are 2.113 and 1.5124 in these waveguides, indicating different manipulations for two orthogonal polarization modes. Particularly, even in the width range from 240 to 400 nm, no phase matching geometry for TM mode can be obtained.

The mode properties of conventional SWGs without Ag layer with the same pitch and duty cycle are shown in Fig. 3f. It is found that in PSWG, the  $n_{\text{eff}}$  difference between TE mode and TM mode is more pronounced than the one in conventional SWG. Therefore, the interaction of TM modes between silicon waveguide and PSWG will be much weaker by employing PSWG as the coupling intermediary.

According to the supermode theory, the coupling length  $L_c$  between silicon waveguide and PSWG can be calculated as [26],

$$L_c = \frac{\lambda_0}{2(n_{\text{even}} - n_{\text{odd}})} \tag{1}$$

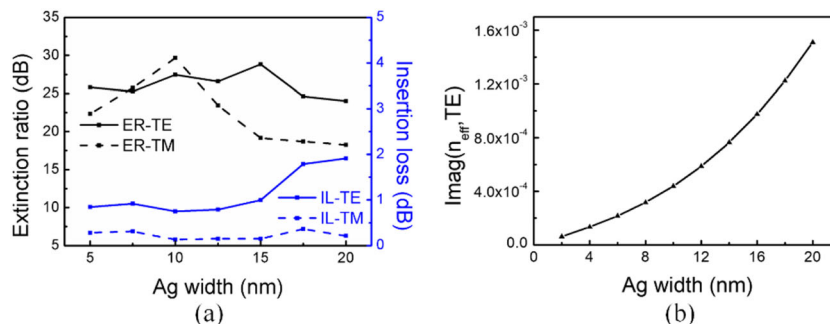
where  $\lambda_0 = 1.55$   $\mu\text{m}$  and  $n_{\text{even}}$  and  $n_{\text{odd}}$  are the real parts of the effective refractive indices of the two supermodes in the coupling region respectively. With  $w_2 = 355$  nm and  $w_1 = 250$  nm, the estimated  $L_c$  is  $\sim 3.2$   $\mu\text{m}$ .

### Results and Discussion

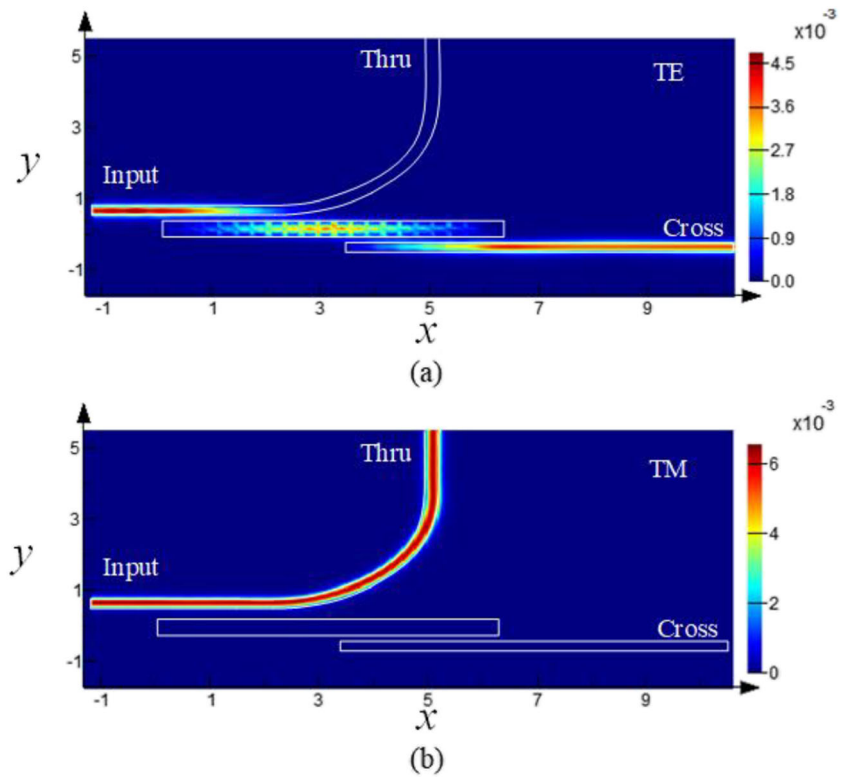
The performances of the device are further verified by three-dimensional finite-difference time-domain (FDTD) method. In order to investigate the impacts of waveguide parameters on the performance, we firstly explored the influence of coupling length  $L_c$  on ER and IL of the proposed device. As shown in Fig. 4, it can be found that TM mode is more sensitive to the effect of  $L_c$  on ER than TE mode while IL of these two modes is nearly immune to  $L_c$  variation. The optimum coupling length is 2.1  $\mu\text{m}$ , which is slightly different from the result calculated by Eq. (1). This can be explained by the fact that mode coupling is still in progress in the bending region. The coupled TE mode power may couple back to the Thru port and consequently degrading the ER.

The wavelength dependence of the PBS performance is demonstrated in Fig. 5. The ER and IL of TE (TM) mode are 27.5 (30) dB and 0.75 (0.13) dB respectively at a wavelength of 1550 nm. Remarkably, the ER of TE mode keeps higher than 27 dB from 1500 to 1600 nm wavelength regime. For TM mode, an ER higher than 21 dB can be obtained covering C-band. Within the investigated wavelength range, the IL of TM mode is lower comparing to TE mode. This is attributed to the fact that TE mode experiences field coupling two times.

**Fig. 6** a ER and IL in TE mode and TM mode with different Ag widths. b The imaginary part of  $n_{\text{eff}}$  of TE mode at different widths of Ag



**Fig. 7** Beam propagation profiles of the TE (a) and TM (b) mode inputs along the PBS with  $w_2 = 355$  nm and  $L_c = 2.1$   $\mu\text{m}$



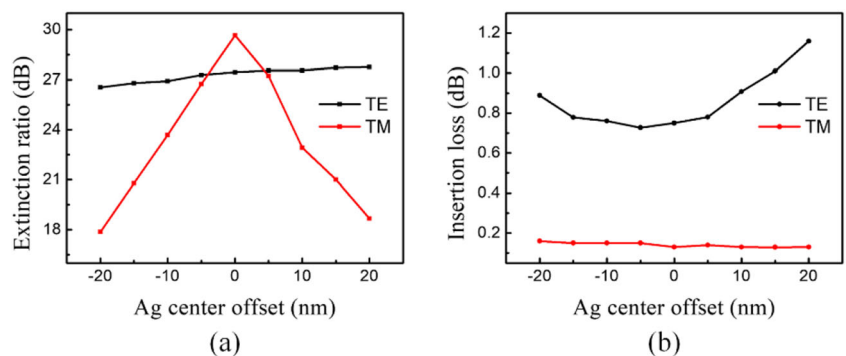
Next, the fabrication tolerances of the proposed PBS are investigated with the variations of the Ag widths ( $t$  in Fig. 1), Ag position offset, and the widths of the silicon waveguide and PSWG, respectively. Figure 6a exhibits the correlation between PBS performance and Ag width. Although the ER of PBS varies with Ag width, it is substantially higher than 18 (24) dB, and the ILs can always keep below 2 (0.3) dB for the TM (TE) mode. The impacts of Ag width on the performance can be attributed to two aspects. Firstly, a change in the Ag width can induce phase mismatch between two TE modes. Secondly, thicker Ag could induce higher propagation loss, Fig. 6b illustrates the imaginary part of  $n_{\text{eff}}$  of the TE mode under different Ag width.

Figure 7 shows the field propagation performances in the proposed PBS. It can be noted from Fig. 4a that, when a TE

mode is launched at input, it can completely couple to PSWG firstly and then to Cross port. It can also be observed from Fig. 7b that, when launching a TM mode, it will propagate along the silicon waveguide and directly output at Thru port. Therefore, the two modes are well separated and an efficient PBS is realized by using the TWDC. It is worth mentioning that compared with PBS using SWG only [20], the addition of Ag shortens the coupling region by more than 30%.

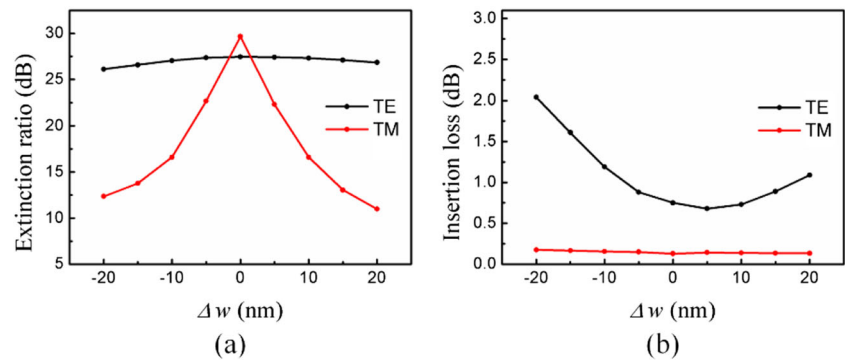
In practical fabrication, the Ag thin film can diverge from the middle of PSWG. The impact of the possible offset of the Ag position was simulated as well. As Fig. 8 shows, the ER of TE mode can be maintained at a relatively high level (about 27 dB) with Ag position offset, while the ER of TM is more sensitive. On the contrary, the IL of TM mode keeps nearly constant and the IL variation of TE mode is more drastic. This

**Fig. 8** a ER and b IL in two modes at different positions of Ag





**Fig. 9** The relationship between ER (a) and IL (b) of two orthogonal modes and the width variation ( $\Delta w$ ) of silicon waveguide and PSWG



can be explained by the fact that the TM mode cannot couple to the PSWG so the TE mode can maintain a high ER. On the contrary, the Ag position offset will induce phase mismatch resulting in incomplete coupling and increasing the IL. Overall, it is better to maintain the Ag offset smaller than 15 nm.

Since width is typically less well-controlled in device fabrication, depending on lithography. Such impacts (by changing  $w_1$ ,  $w_2$  and  $w_3$ , simultaneously) are summarized in Fig. 9. For TE mode, the ER can be kept above 26 dB, indicating large tolerance to width variation. As  $\Delta w$  decrease (expressed by negative value) or increases (expressed by positive value), the gap between waveguides becomes wider or narrower, so the optimized coupling length of TE mode will diverge from 2.1  $\mu\text{m}$  and therefore degrading the ER of TM, while the ER and IL for both modes can be higher than 10 dB and lower than 2 dB within  $\pm 20$  nm of  $\Delta w$ .

Overall, since only TE mode coupling occurs between PSWG and silicon waveguide, the size variation has a relatively large influence on this mode. On the contrary, since the phase mismatch between TM modes is quite large, the TM mode power appearing in both ports is almost independent of size changes. Considering a rough 10-nm resolution can be usually guaranteed for electron beam lithography, the device fabrication tolerance is still acceptable.

## Conclusion

In conclusion, we have designed a TWDC-based PBS in which a PSWG is employed to provide large birefringence two orthogonally polarized modes. The PSWG can induce strong coupling for TE mode with negligible impacts on TM mode leading to effective separation between them. From results, an IL lower than 1 dB (TE) and 0.18 dB (TM), together with an ER higher than 30 dB (TE) and 27 dB (TM) covering the entire C-band, can be achieved in a compact device with only  $\sim 4$   $\mu\text{m}$ . The device has potential application prospects in the field of polarization-sensitive integrated photonic circuits.

**Funding Information** This work was supported by the National Natural Science Foundation of China under grant 61605179; the Wuhan Science and Technology Bureau under grant 2018010401011297; the Fundamental Research Funds for the Central Universities, China University of Geosciences (Wuhan) under grants 162301132703, G1323511794, and CUG2018JM16; and the Experimental Technology Research Funds under grant SJ-201816.

## References

- Xiao J, Guo Z (2018) Ultracompact polarization-insensitive power splitter using subwavelength gratings. *IEEE Photon Technol Lett* 30:529–532
- Saidani N, Belhadj W, AbdelMalek F, Bouchriha H (2012) Detailed investigation of self-imaging in multimode photonic crystal waveguides for applications in power and polarization beam splitters. *Opt Commun* 285:3487–3492
- Xu Y, Xiao J, Sun X (2015) Proposal for compact polarization splitter using asymmetrical three-guide directional coupler. *IEEE Photon Technol Lett* 27:654–657
- Lu Z, Wang Y, Zhang F, Jaeger NAF, Chrostowski L (2015) Wideband silicon photonic polarization beamsplitter based on point-symmetric cascaded broadband couplers. *Opt Express* 23:29413–29422
- Guan X, Wu H, Shi Y, Dai D (2014) Extremely small polarization beam splitter based on a multimode interference coupler with a silicon hybrid plasmonic waveguide. *Opt Lett* 39:259–262
- Guan X, Chen P, Chen S, Xu P, Shi Y, Dai D (2014) Low-loss ultracompact transverse-magnetic-pass polarizer with a silicon sub-wavelength grating waveguide. *Opt Lett* 39:4514–4517
- Qiu H, Su Y, Yu P, Hu T, Yang J, Jiang X (2015) Compact polarization splitter based on silicon grating-assisted couplers. *Opt Lett* 40:885–1887
- Zhang Y, He Y, Wu J, Jiang X, Liu R, Qiu C, Jiang X, Yang J, Tremblay C, Su Y (2016) High-extinction-ratio silicon polarization beam splitter with tolerance to waveguide width and coupling length variations. *Opt Express* 24:6586–6593
- Bock PJ, Cheben P, Schmid JH, Lapointe J, Del age A, Janz S, Hall TJ (2010) subwavelength grating periodic structures in silicon-on-insulator: a new type of microphotonic waveguide. *Opt Express* 18:20251–20262
- Halir R, Bock PJ, Cheben P, Ortega-Mo nux A, Alonso-Ramos C, Schmid JH, Lapointe J, Xu D, Wang iemert-P erez JG, Molina-Fernandez I, Janz S (2015) Waveguide sub-wavelength structures: a review of principles and applications. *Laser Photonics Rev* 9:25–49
- Z. Pan, X. Xu, C. Chung, H. Dalir, H. Yan, K. Chen, Y. Wang, B. Jia, and R. T. Chen (2018) High-speed modulator based on electro-

- optic polymer infiltrated subwavelength grating waveguide ring resonator Optical Fiber Communication Conference M2I.2
12. Xu Y, Xiao J (2016) An ultracompact polarization-insensitive silicon-based strip-to-slot power splitter. *IEEE Photon Technol Lett* 28: 536–539
  13. Benedikovic D, Cheben P, Schmid JH, Xu D, Lapointe J, Wang S, Halir R, Ortega-Moñux A, Janz S, Dado M (2014) High-efficiency single etch step apodized surface grating coupler using subwavelength structure. *Laser Photonics Rev* 8:L93–L97
  14. Guo Z, Xiao J (2017) Ultracompact silicon-based polarization beam splitter using subwavelength gratings. *IEEE Photon Technol Lett* 29:1800–1803
  15. Xu Y, Xiao J (2016) Compact and high extinction ratio polarization beam splitter using subwavelength grating couplers. *Opt Lett* 41: 773–776
  16. Gramotnev DK, Bozhevolnyi SI (2010) Plasmonics beyond the diffraction limit. *Nat Photonics* 4:83–91
  17. Guan X, Wu H, Shi Y, Wosinski L, Dai D (2013) Ultracompact and broadband polarization beam splitter utilizing the evanescent coupling between a hybrid plasmonic waveguide and a silicon nanowire. *Opt Lett* 38:3005–3008
  18. Dai D, Bauters J, Bowers JE (2012) Passive technologies for future large-scale photonic integrated circuits on silicon: polarization handling, light non-reciprocity and loss reduction. *Light Sci Appl* 1: 500–505
  19. Chee J, Zhu S, Lo GQ (2012) CMOS compatible polarization splitter using hybrid plasmonic waveguide. *Opt Express* 20:25345–25355
  20. Huang T, Xie Y, Wu Y, Cheng Z, Zeng S, Ping PS (2019) Compact polarization beam splitter assisted by subwavelength grating in triple-waveguide directional coupler. *Appl Opt* 58:2264–2268
  21. Liu L, Deng Q, Zhou Z (2016) Manipulation of beat length and wavelength dependence of a polarization beam splitter using a subwavelength grating. *Opt Lett* 41:5126–5129
  22. Sarmiento-Merenguel JD, Ortega-Moñux A, Fédéli JM, Wangüemert-Pérez JG, Alonso-Ramos C, Duran-Valdeiglesias E, Cheben P, Molina-Fernandez I, Halir R (2016) Controlling leakage losses in subwavelength grating silicon metamaterial waveguides. *Opt Lett* 41:3443–3446
  23. Palik ED (1991) *Handbook of Optical Constants of Solids*. Academic Press, New York
  24. Chen LR, Wang J, Naghdi B, Glesk I (2019) Subwavelength grating waveguide devices for telecommunications applications. *IEEE J Sel Top Quantum Electron* 25:1–1
  25. Huang Y, Song J, Luo X, Liow TY, Lo GQ (2014) CMOS compatible monolithic multi-layer Si<sub>3</sub>N<sub>4</sub> on SOI platform for low-loss high performance silicon photonics dense integration. *Opt Express* 22: 21859–21865
  26. Donnelly J (1986) Limitations on power-transfer efficiency in three-guide optical couplers. *IEEE J Quantum Electron* 22:610–616

**Publisher's Note** Springer Nature remains neutral with regard to jurisdictional claims in published maps and institutional affiliations.